

Strong-field effects in massive scalar-tensor gravity for slowly spinning neutron stars and application to X-ray pulsar pulse profiles

Rui Xu,^{1,*} Yong Gao,^{2,1} and Lijing Shao^{1,3,†}

¹*Kavli Institute for Astronomy and Astrophysics, Peking University, Beijing 100871, China*

²*Department of Astronomy, School of Physics, Peking University, Beijing 100871, China*

³*National Astronomical Observatories, Chinese Academy of Sciences, Beijing 100012, China*

(Dated: September 10, 2020)

Neutron stars (NSs) in scalar-tensor (ST) theories of gravitation can acquire scalar charges and generate distinct spacetimes from those in General Relativity (GR) through the celebrated phenomenon of spontaneous scalarization. Taking on an ST theory with the mass term of the scalar field, we determine the theory parameter space for spontaneous scalarization by investigating the linearized scalar field equation. Then the full numerical solutions for slowly rotating NSs are obtained and studied in great detail. The resulted spacetime is used to calculate test-particle geodesics. The lightlike geodesics are used to construct the profile of X-ray radiation from a pair of hot spots on the surface of scalarized NSs, which potentially can be compared with the data from the Neutron star Interior Composition Explorer (NICER) mission for testing the ST theory.

I. INTRODUCTION

Gravitational effects are solely described by the metric tensor in General Relativity (GR). The simplest extension to its field content is adding in a real scalar field, forming a scalar-tensor (ST) theory of gravitation [1–3]. Depending on how the scalar couples with the metric as well as conventional matters, the solutions of an ST theory can be identical to or very different from those of GR. It is particularly interesting to study the ST theories that produce identical or close enough solutions to those of GR in the weak-field regime so that they pass all the Solar-system tests as GR does, but that become sufficiently distinct from GR in the strong-field regime to compete with it [2, 4]. In this work we will focus on neutron stars (NSs) in this kind of ST theories. One well-studied class of ST theories are characterized by the phenomenon called *spontaneous scalarization*, first discovered and explored by Thibault Damour and Gilles Esposito-Farèse for NSs [5–8].

Spontaneous scalarization for NSs can be physically understood as a result of *phase transition*, where for example, the control parameter of the system can be taken as the baryonic mass of the NS [6, 7] and Landau’s phase transition theory can be naturally applied [9]. From the mathematical point of view, it corresponds to the parameter space (both of the ST theories and of the NS under study) in which the system acquires two distinct solutions: one has the GR metric together with a trivial scalar and the other has a nontrivial scalar with a metric different from GR. The latter is energetically favored thus represents the physical solution.

The existence of spontaneous scalarization requires conditions on both the ST theory and the NS. First, the theory must possess nonminimal couplings between the scalar field and the metric. Then, there are restrictions on the theory parameters and the system parameters. These two points are well illustrated in Refs. [5, 6] with numerical solutions to the widely known ST theory proposed by Damour and Esposito-Farèse

(hereafter, DEF theory). The nonminimal coupling in the Jordan frame can be transformed to a conformal coupling in the Einstein frame between the metric and matter fields (see e.g. Ref. [8]). In the DEF theory, the conformal coupling is described by an exponential function of the square of the scalar field, namely $A(\varphi) = \exp(\beta\varphi^2/2)$. The exponential function decays as the scalar field increases due to a negative coefficient β in front of the square of the scalar field. The theory parameter β needs to be less than about -4 to have spontaneous scalarization for NSs, and simultaneously, for each valid β the solutions of spontaneous scalarization occupy an interval of the system parameter, which, when taken as the compactness of the system C , is around $1/|\beta|$ [5, 7, 10].

When the theory parameter $\beta < -4$ naturally takes values of order unity, NSs coincidentally become the easiest objects to scalarize in the DEF theory as their compactnesses match right to the required system compactness $C \sim 1/|\beta|$. This makes the observations of pulsars, which are magnetized rotating NSs emitting electromagnetic radiation, perfectly suitable to test such a theory. Based on the gravitational radiation formulae derived from the post-Newtonian approximation [3], as well as numerical descriptions of scalarized NSs [6], observations of decays in pulsar orbits due to gravitational-wave (GW) damping have been used to constrain β [11–15]. The most stringent constraint coming from a combination of multiple binary pulsars indicates $\beta > -4.35$ for almost all supranuclear equations of state (EOSs) [13–18].

As the theory parameter space shrinks significantly for the DEF theory, considering a massive scalar instead of a massless one as that in the DEF theory becomes appealing. Due to the quick Yukawa-type decrease of the scalar field caused by its mass, the scalar contribution to GW radiation is automatically suppressed in massive ST theories. Hence, the precise pulsar-timing observations still do not exclude much of the theory parameter space of massive ST theories yet. In addition, massless ST theories of such kind have problems to simultaneously account for the right behavior in cosmology after the matter-dominated era [19, 20], while preserving the strong-field scalarization of NSs. The whole Universe would have been scalarized when the mass of the scalar is strictly

* Corresponding author: xuru@pku.edu.cn

† Corresponding author: lishao@pku.edu.cn

zero, and a massive scalar is a natural saviour to evade the scalarization of the whole Universe [10, 21, 22]. Moreover, another motivation from cosmology for considering massive ST theories is that such models are natural candidates for dark matter as the massive scalar only interacts with baryonic matter gravitationally (e.g., see Refs. [23, 24]).

Numerical solutions of spontaneous scalarization for single spherical NSs have been constructed in the massive version of the DEF theory with a constant scalar mass in the Einstein frame [10, 25]. As the Jordan frame, where conventional matters do not couple with the scalar directly, is usually considered as the physical frame whose metric can be measured by clocks and meter sticks, we consider a massive ST theory with a constant scalar mass in this frame. The conformal transformation connecting the two frames depends on the scalar field, therefore a constant scalar mass in one frame is no longer constant in the other. We also point out that there is another difference between the massive ST theory studied in this work and the DEF theory with a mass term. The function of the scalar that describes the conformal coupling takes a rational form instead of the exponential form in the DEF theory. This is an important check of a different choice because, as numerically shown in Ref. [5], strong-field effects probe a large segment of the conformal coupling function, not only in the neighbour around $\varphi \ll 1$.¹

Our work contains the full numerical solutions of single scalarized NSs and an application of the solutions in constructing the X-ray pulse profiles of slowly rotating scalarized NSs. In solving NSs numerically, we investigate the linearized scalar field in detail and obtain the theory parameter space for spontaneous scalarization to happen. This follows the simple model of the linearized scalar equation in Ref. [5], with which Damour and Esposito-Farèse showed that the scalar field is amplified when β is negative to explain the occurrence of spontaneous scalarization. In applying the numerical solutions to the pulse profile of X-ray pulsars, we review the prescription in Ref. [26] and generalize their results to any spherical static spacetime. Explicit examples are illustrated for the radius, mass, moment of inertia of scalarized NSs, as well as pulse profiles of X-ray pulsars.

The organization of this paper is as follows. The equations to be solved are derived from the action of the theory in Sec. II by putting forward a metric ansatz for a slowly rotating perfect-fluid NS. Section III A demonstrates the occurrence of spontaneous scalarization and settles the valid parameter space using the linearized scalar equation, while Sec. III B presents the numerical results for the nonlinear problem. Then, in Sec. IV A, geodesics around scalarized NSs are discussed, and in Sec. IV B, lightlike trajectories are used to calculate the X-ray flux from a pair of hot spots on the surface of a slowly rotating NS following Ref. [26]. To conclude the paper, a summary is provided in Sec. V. Appendix A exhibits the series expansion of the linearized scalar equation at the center of the star.

Throughout this work, we use the geometrized unit system where $G = c = 1$ except when the units are written out explicitly, and the convention of the metric is $(-, +, +, +)$.

II. SETUP OF THE PROBLEM

Writing in the Jordan frame, we study the ST theory given by the action [6, 27]

$$S = \frac{1}{16\pi} \int d^4x \sqrt{-\tilde{g}} \left(\tilde{R} - \tilde{g}^{\mu\nu} \partial_\mu \Phi \partial_\nu \Phi - U(\Phi) + \xi \tilde{R} \Phi^2 \right) + S_m[\Psi_m; \tilde{g}_{\mu\nu}], \quad (1)$$

where the tildes denote the metric and the metric-related quantities in the Jordan frame, while Φ is specifically designated as the scalar field in this frame. Conventional matters are represented by Ψ_m collectively in the matter action S_m , which does not contain the scalar field Φ . To have a massive scalar field, the scalar potential takes the form

$$U(\Phi) = \left(\frac{2\pi}{\lambda_\Phi} \right)^2 \Phi^2, \quad (2)$$

where we have omitted higher-order interactions like the Φ^4 term (e.g., see Refs. [27, 28]). The constant λ_Φ has dimension of length so that the mass of the scalar can be defined as

$$m_\Phi = \frac{h}{\lambda_\Phi}, \quad (3)$$

where h is the Planck constant that has dimension of length squared in the geometrized unit system. The nonminimal coupling term in Eq. (1), $\xi \tilde{R} \Phi^2$, is taken from inflationary models where the inflaton is a single scalar with ξ being the dimensionless coupling constant (e.g., see Refs. [29–31]).

The field equations are obtained by taking variations with respect to $\tilde{g}_{\mu\nu}$ and Φ . They are

$$\left(1 + \xi \Phi^2 \right) \tilde{R}_{\mu\nu} = 8\pi \left(\tilde{T}_{\mu\nu} - \frac{1}{2} \tilde{g}_{\mu\nu} \tilde{T} \right) + \partial_\mu \Phi \partial_\nu \Phi + \frac{1}{2} \tilde{g}_{\mu\nu} U(\Phi) + \xi \left(\tilde{D}_\mu \tilde{D}_\nu + \frac{1}{2} \tilde{g}_{\mu\nu} \tilde{\square} \right) \Phi^2, \quad (4)$$

and

$$\left(\tilde{\square} + \xi \tilde{R} \right) \Phi = \frac{1}{2} \frac{dU}{d\Phi}, \quad (5)$$

where the energy-momentum tensor for conventional matters is

$$\tilde{T}_{\mu\nu} \equiv - \frac{2}{\sqrt{-\tilde{g}}} \frac{\delta S_m}{\delta \tilde{g}^{\mu\nu}}, \quad (6)$$

and the d'Alembert operator is $\tilde{\square} = \tilde{g}^{\mu\nu} \tilde{D}_\mu \tilde{D}_\nu$ with \tilde{D}_μ being the covariant derivative associated with the metric $\tilde{g}_{\mu\nu}$.

Attempts to solve Eqs. (4) and (5) require metric ansatzes in the Jordan frame. But we prefer to use a metric ansatz in

¹ Damour and Esposito-Farèse [5] demonstrated this point using $A(\varphi) = \exp(-3\varphi^2)$ and $A(\varphi) = \cos(\sqrt{6}\varphi)$ as examples.

the Einstein frame, because equations in the Einstein frame are simpler. With the conformal transformation

$$\tilde{g}_{\mu\nu} \equiv A^2(\Phi)g_{\mu\nu} \equiv \frac{1}{1 + \xi\Phi^2}g_{\mu\nu}, \quad (7)$$

and a field redefinition of the scalar satisfying

$$\left(\frac{d\varphi}{d\Phi}\right)^2 \equiv W(\Phi) \equiv \frac{3}{4} \left(\frac{2\xi\Phi}{1 + \xi\Phi^2}\right)^2 + \frac{1}{2} \frac{1}{1 + \xi\Phi^2}, \quad (8)$$

the action (1) as well as the field equations (4) and (5) can be transformed into the Einstein frame. They read

$$S = \frac{1}{16\pi} \int d^4x \sqrt{-g} \left(R - 2g^{\mu\nu} \partial_\mu \varphi \partial_\nu \varphi - V(\varphi) \right) + S_m \left[\Psi_m; A^2(\varphi)g_{\mu\nu} \right], \quad (9)$$

$$R_{\mu\nu} = 2\partial_\mu \varphi \partial_\nu \varphi + \frac{1}{2}g_{\mu\nu} V(\varphi) + 8\pi \left(T_{\mu\nu} - \frac{1}{2}g_{\mu\nu} T \right), \quad (10)$$

and

$$\square \varphi = \frac{1}{4} \frac{dV(\varphi)}{d\varphi} - 4\pi \frac{d \ln A(\varphi)}{d\varphi} T, \quad (11)$$

where the scalar potential and the d'Alembert operator in the Einstein frame are $V(\varphi) = A^4(\varphi)U(\Phi(\varphi))$ and $\square = g^{\mu\nu}D_\mu D_\nu$, respectively. The energy-momentum tensor for conventional matters in the Einstein frame is

$$T_{\mu\nu} \equiv -\frac{2}{\sqrt{-g}} \frac{\delta S_m}{\delta g^{\mu\nu}} = A^2 \tilde{T}_{\mu\nu}. \quad (12)$$

In the above equations, the metric and the metric-related quantities in the Einstein frame are written without any decoration, and the scalar field in the Einstein frame is denoted as φ specifically. For our purpose, we will employ the Einstein field equations (10) rather than (4) for it is simpler, but the scalar equation (5) rather than (11) to avoid solving the relation between Φ and φ from the differential equation (8). Such a treatment is proper as long as we take care of the transformations throughout the calculation.

Before we proceed with a metric ansatz, we point out that the nonminimal coupling in Eq. (1) can be matched to that in the DEF theory when the scalar field is small. In fact, the coupling function $A(\varphi)$ in the DEF theory is [6]

$$A(\varphi) = \exp\left(\frac{1}{2}\beta\varphi^2\right) = 1 + \frac{1}{2}\beta\varphi^2 + O(\varphi^4), \quad (13)$$

while the coupling function $A(\Phi(\varphi))$ defined in Eq. (7) becomes

$$A(\Phi(\varphi)) = 1 - \frac{\xi}{2}\Phi^2 + O(\Phi^4) = 1 - \xi\varphi^2 + O(\varphi^4), \quad (14)$$

when the scalar field is small. Therefore, if [6]

$$\xi = -\frac{1}{2}\beta, \quad (15)$$

the theory studied here is equivalent to the massive DEF theory in the regime of a weak scalar field.

Now following Ref. [6], we use the metric ansatz

$$ds^2 = g_{\mu\nu}dx^\mu dx^\nu = -e^{\nu(\rho)} dt^2 + e^{\mu(\rho)} d\rho^2 + \rho^2 d\theta^2 + \rho^2 \sin^2 \theta (d\phi + (\omega(\rho, \theta) - \Omega)dt)^2, \quad (16)$$

to simplify the field equations (5) and (10). The line element is written in the Einstein frame with coordinates (t, ρ, θ, ϕ) and unknown functions $\mu(\rho)$, $\nu(\rho)$, $\omega(\rho, \theta)$. The metric components in the Jordan frame can be obtained via Eq. (7). The angular velocity of the star, Ω , assumed to be constant, is introduced as the asymptotic value of $\omega(\rho, \theta)$ when $\rho \rightarrow \infty$.

The fluid variables, on the other hand, are conventionally written in the Jordan frame, namely that the energy-momentum tensor in the Jordan frame takes the form

$$\tilde{T}^{\mu\nu} = (\tilde{\epsilon} + \tilde{p})\tilde{u}^\mu \tilde{u}^\nu + \tilde{g}^{\mu\nu} \tilde{p}, \quad (17)$$

where $\tilde{\epsilon}$ and \tilde{p} are related by the EOS, and the 4-velocity \tilde{u}^μ is

$$\tilde{u}^\mu = \frac{1}{\sqrt{-\tilde{g}_{tt} - 2\Omega\tilde{g}_{t\phi} - \Omega^2\tilde{g}_{\phi\phi}}} (1, 0, 0, \Omega). \quad (18)$$

Confined to slowly rotating NSs and keeping only the linear terms of ω and Ω in the field equations, we find that the fluid variables, $\tilde{\epsilon}$, \tilde{p} , and the scalar field, Φ , are functions of the radial coordinate ρ alone [32], and that $\omega(\rho, \theta)$ remarkably obeys an equation in the same form as that in the massless case in Ref. [6]:

$$\begin{aligned} & \frac{1}{\rho^4} e^{-\frac{\mu-\nu}{2}} \frac{\partial}{\partial \rho} \left(\rho^4 e^{-\frac{\mu+\nu}{2}} \frac{\partial \omega}{\partial \rho} \right) + \frac{1}{\rho^2 \sin^3 \theta} \frac{\partial}{\partial \theta} \left(\sin^3 \theta \frac{\partial \omega}{\partial \theta} \right) \\ & = \frac{16\pi G}{c^4} A^4 (\tilde{\epsilon} + \tilde{p}) \omega, \end{aligned} \quad (19)$$

with the coupling function A defined in Eq. (7) and no contribution from the scalar potential U . Equation (19) allows a separation of variables and additionally implies that ω is independent of θ when the asymptotic behavior of ω is taken into account [32, 33]. Therefore, ω is also a function of the radial coordinate ρ alone, and the field equations (5) and (10) become a group of ordinary differential equations (ODEs).

With the change of variable

$$e^\mu \equiv \left(1 - \frac{2m(\rho)}{\rho} \right)^{-1}, \quad (20)$$

the ODEs written out explicitly are

$$\begin{aligned}
m' &= 4\pi\rho^2 A^4 \tilde{\epsilon} + \frac{1}{2}\rho(\rho - 2m)W\Phi'^2 + \frac{1}{4}\rho^2 A^4 U, \\
\nu' &= \frac{8\pi\rho^2 A^4 \tilde{p}}{\rho - 2m} + \frac{2m}{\rho(\rho - 2m)} + \rho W\Phi'^2 - \frac{1}{2}\frac{\rho^2}{(\rho - 2m)}A^4 U, \\
\omega'' &= \frac{4\pi\rho}{\rho - 2m}A^4(\tilde{\epsilon} + \tilde{p})(\rho\omega' + 4\omega) + \left(\rho W\Phi'^2 - \frac{4}{\rho}\right)\omega', \\
\tilde{p}' &= -(\tilde{\epsilon} + \tilde{p})\left(\frac{4\pi\rho^2 A^4 \tilde{p}}{\rho - 2m} + \frac{m}{\rho(\rho - 2m)}\right. \\
&\quad \left. + \frac{1}{2}\rho W\Phi'^2 + \frac{A'}{A} - \frac{1}{4}\frac{\rho^2}{(\rho - 2m)}A^4 U\right), \\
\Phi'' &= \frac{4\pi\rho A^4}{\rho - 2m}\left(\rho(\tilde{\epsilon} - \tilde{p})\Phi' + \frac{1}{WA}\frac{dA}{d\Phi}(\tilde{\epsilon} - 3\tilde{p})\right) \\
&\quad - \frac{W'\Phi'}{2W} - \frac{2(\rho - m)}{\rho(\rho - 2m)}\Phi' \\
&\quad + \frac{\rho A^4}{\rho - 2m}\left(\frac{1}{2}\rho U\Phi' + \left(\frac{U}{A}\frac{dA}{d\Phi} + \frac{1}{4}\frac{dU}{d\Phi}\right)\frac{1}{W}\right), \quad (21)
\end{aligned}$$

where the primes denote derivatives with respect to the radial coordinate ρ , and U , A and W are functions of Φ given in Eqs. (2), (7) and (8). We point out that the above set of equations recover those in Refs. [6, 10, 25, 27, 28] if U , A and W take appropriate forms corresponding to the coupling functions and the scalar potentials there, and the transformation between the Einstein frame and the Jordan frame is accounted for properly. The group of equations in (21) is completed by adding in the EOS of NSs.

A preliminary inspection of the equations in (21) reveals that the coupled equations are those of m , \tilde{p} and Φ . The function ν can be integrated out with the condition of asymptotic flatness once m , \tilde{p} and Φ are known. The function ω can be scaled by an arbitrary factor as its equation is homogeneous. In addition, to guarantee $\omega''|_{\rho=0}$ to be finite, we have $\omega'|_{\rho=0} = 0$. Therefore, numerical solutions to the group of equations in (21) only rely on the initial conditions of m , \tilde{p} and Φ at $\rho = 0$, which are

$$m|_{\rho=0} = 0, \quad \tilde{p}|_{\rho=0} = \tilde{p}_c, \quad \Phi|_{\rho=0} = \Phi_c, \quad \Phi'|_{\rho=0} = 0. \quad (22)$$

In conclusion, there are two system parameters, the central pressure \tilde{p}_c and the central scalar field Φ_c , that can be adjusted in searching for numerical solutions of spontaneous scalarization, given a theory with parameters ξ and m_Φ .

From the asymptotic behavior of m and ω , two important global quantities, the ADM mass M and the angular momentum J , can be extracted. Specifically speaking, when $\rho \rightarrow \infty$ we have

$$\begin{aligned}
g_{\rho\rho} &= \left(1 - \frac{2m(\rho)}{\rho}\right)^{-1} \rightarrow 1 + \frac{2M}{\rho}, \\
g_{t\phi} &= (\omega - \Omega)\rho^2 \sin^2 \theta \rightarrow -\frac{2J \sin^2 \theta}{\rho}, \quad (23)
\end{aligned}$$

indicating

$$M = m|_{\rho \rightarrow \infty}, \quad J = \frac{1}{6}\rho^4 \omega'|_{\rho \rightarrow \infty}. \quad (24)$$

The moment of inertia of the star can then be calculated via

$$I = \frac{J}{\Omega} = \frac{1}{6}\frac{\rho^4 \omega'}{\omega}\Big|_{\rho \rightarrow \infty}. \quad (25)$$

We point out that as $\Phi \rightarrow 0$ when $\rho \rightarrow \infty$, the coupling function A becomes unity so that the Einstein frame and the Jordan frame coincide. Hence, the ADM mass M , the angular momentum J , and the moment of inertia I are independent of the frame choice.

III. SOLUTIONS OF SPONTANEOUS SCALARIZATION

In this section, we investigate the NS solutions from the action (1) in a linearized limit (Sec. III A) and in the fully nonlinear problem (Sec. III B).

A. Linearized scalar field equation

As a warm-up, we deal with the linearized version of the scalar field equation in (21). This is sufficient to show how spontaneous scalarization occurs and yields restrictions on the parameter space of the theory for it to happen. By taking

$$A^2 = 1 - \xi\Phi^2 + O(\Phi^4), \quad W = \frac{1}{2} + O(\Phi^2),$$

and keeping only the linear terms of Φ , Φ' and Φ'' , the scalar equation in (21) simplifies to

$$\begin{aligned}
\Phi'' &= \frac{4\pi\rho^2}{\rho - 2m}(\tilde{\epsilon} - \tilde{p})\Phi' - \frac{2(\rho - m)}{\rho(\rho - 2m)}\Phi' \\
&\quad - \frac{8\pi\xi\rho}{\rho - 2m}(\tilde{\epsilon} - 3\tilde{p})\Phi + \left(\frac{2\pi}{\lambda_\Phi}\right)^2 \frac{\rho}{\rho - 2m}\Phi, \quad (26)
\end{aligned}$$

where we assume that m , $\tilde{\epsilon}$ and \tilde{p} take GR results and are known. Realistic EOSs of NSs can be used to obtain GR solutions of m , $\tilde{\epsilon}$ and \tilde{p} [34]. For demonstration purpose, we currently employ a toy EOS

$$\tilde{\epsilon} = \text{const.}, \quad (27)$$

which has the advantage to have analytical expressions of m and \tilde{p} , in order to show how spontaneous scalarization occurs.

Using a characteristic length l_0 to define the dimensionless quantities

$$x \equiv \frac{\rho}{l_0}, \quad y \equiv \frac{m}{l_0}, \quad u \equiv 4\pi l_0^2 \tilde{\epsilon}, \quad v \equiv 4\pi l_0^2 \tilde{p}, \quad a \equiv \frac{2\pi l_0}{\lambda_\Phi}, \quad (28)$$

turns out to be handy. The dimensionless version of Eq. (26) can be written as

$$\begin{aligned}
\left(1 - \frac{2y}{x}\right)\Phi_{xx} + \left(\frac{2}{x}\left(1 - \frac{y}{x}\right) - (u - v)x\right)\Phi_x \\
+ (2\xi(u - 3v) - a^2)\Phi = 0, \quad (29)
\end{aligned}$$

where the subscript x denotes the derivative with respect to x . In the case of a constant $\tilde{\epsilon}$, it is convenient to take the characteristic length as

$$l_0 = \sqrt{\frac{3}{8\pi\tilde{\epsilon}}}, \quad (30)$$

and then the GR solution for m and \tilde{p} can be written as

$$\begin{aligned} y &= \frac{1}{2}x^3, \\ v &= \frac{3\eta\sqrt{1-x^2}-1}{2(1-\eta\sqrt{1-x^2})}, \end{aligned} \quad (31)$$

where η is an integral constant that fixes the parameters of the star. For example, the dimensionless radius of the star is

$$x_s = \sqrt{1 - \frac{1}{9\eta^2}}, \quad (32)$$

and the compactness of the star is

$$C = \frac{y}{x}\Big|_{x=x_s} = \frac{1}{2}\left(1 - \frac{1}{9\eta^2}\right). \quad (33)$$

Assuming $\eta \in (1/3, 1)$, the compactness C increases with η from 0 to 4/9.

Though equipped with analytical expressions of y , u and v , the analytical solution to Eq. (29) is difficult to find. Therefore we take a semi-analytical approach. Starting at the center of the star, for given values of C , ξ and a , we find that the requirement of a finite $\Phi|_{x=0}$ fixes the solution up to a scaling constant (see Appendix A). The scaling constant preserves the ratio of Φ_x to Φ , so the solution is in fact fully determined once we assign $\Phi|_{x=0} = 1$ by taking advantage of the homogeneity of Eq. (29). However, the asymptotic solution of Eq. (29) clearly takes the general form

$$\Phi \rightarrow \frac{\Phi_+}{x}e^{ax} + \frac{\Phi_-}{x}e^{-ax}, \quad (34)$$

where the integral constant Φ_+ must vanish and the integral constant Φ_- must be nonzero for nontrivial physical solutions. For given values of C , ξ and a , this asymptotic condition is generally not satisfied by the already fixed solution obtained through integrating from the center, causing the only solution to be the trivial one: $\Phi = 0$ everywhere.

To find for what values of C , ξ and a , there are nontrivial solutions, we split Eq. (29) into the interior part and the exterior part that match at the surface of the star where $x = x_s$. The interior equation is solved from the center straightforwardly, while the exterior equation is solved from the surface of the star with the shooting method to guarantee $\Phi \rightarrow 0$ at infinity. In applying the shooting method, we fix $\Phi|_{x=x_s} = 1$ and adjust $\Phi_x|_{x=x_s}$ to achieve a vanishingly small Φ at large enough x . The interior and the exterior solutions should match at $x = x_s$, by which we mean that the value of Φ_x/Φ at the surface obtained from the interior solution should equal to that determined by the shooting method in solving the exterior equation.

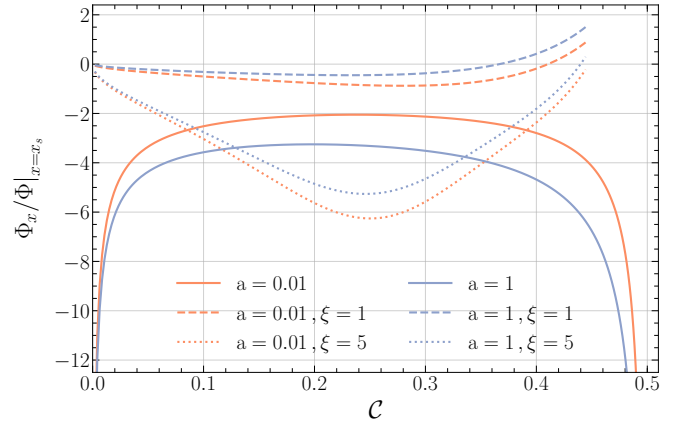


FIG. 1. $\Phi_x/\Phi|_{x=x_s}$ with respect to the compactness C . The solid curves are for the exterior solutions, while the dashed and the dotted curves are for the interior solutions.

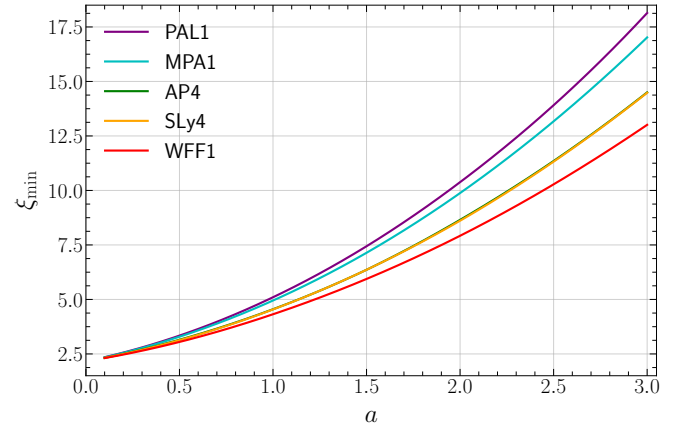


FIG. 2. The minimal value of ξ for spontaneous scalarization versus the dimensionless scalar mass a for five realistic EOSs; see Eq. (35) to convert a to the physical scalar mass m_ϕ . The curves for the EOS AP4 and for the EOS SLy4 largely overlap in the graph.

Varying C , ξ and a , values of Φ_x/Φ on the surface of the star for both interior and exterior solutions are calculated numerically. Figure 1 plots these values with reference to the compactness C for two values of ξ and a to show the following features:

1. The existence of nontrivial solutions demands ξ to be greater than or equal to a critical value $\xi_{\min}(a)$ for a given value of a .
2. When $\xi > \xi_{\min}(a)$ for a given value of a , the nontrivial solutions come up at two values of C .

The relation $\xi_{\min}(a)$ and the two values of C for given $\xi > \xi_{\min}(a)$ define the boundaries of the parameter space for spontaneous scalarization to happen. This is verified in the numerical results for the nonlinear problem in Sec. III B. Figure 1 also suggests that Schwarzschild black holes cannot be scalarized in the theory studied here since Φ_x/Φ at the surface necessary for a nontrivial physical solution diverges when

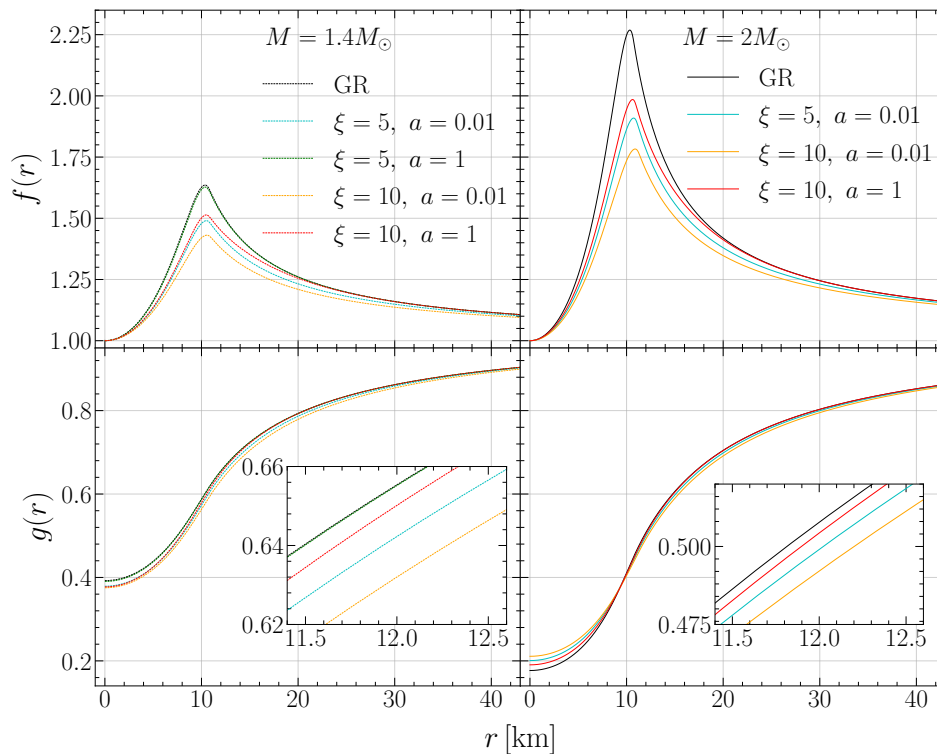


FIG. 3. Representative solutions for the Jordan-frame metric components $g(r)$ and $f(r)$ defined in Eq. (39). EOS AP4 is used in calculation, and the ADM masses of the NSs are chosen to be $1.4 M_\odot$ (left panels) and $2.0 M_\odot$ (right panels).

$C \rightarrow 1/2$; though the EOS in Eq. (27) does not produce black holes, the exterior equation of Eq. (29) still exists if the metric is taken to be the Schwarzschild metric.

The above calculations can be repeated with realistic EOSs of NSs. Dealing with such EOSs hereafter, we take the characteristic length $l_0 = 10$ km, so the scalar mass is

$$m_\Phi = \frac{ah}{2\pi l_0} \approx a \times 1.97 \times 10^{-11} \text{ eV}. \quad (35)$$

Figure 2 plots the relation $\xi_{\min}(a)$ for several realistic EOSs: PAL1, MPA1, AP4, SLy4, and WFF1 [34]. Except for PAL1, all the EOSs are chosen to simultaneously satisfy the observations of two-Solar-mass pulsars [12, 35] and the tidal deformability from the binary NS merger GW170817 [36–38]. The EOS PAL1, representing a stiff EOS excluded by GW170817, is in the list for comparison. For $a \rightarrow 0$, ξ_{\min} is around 2, confirming the critical value of $\beta \sim -4$ in the DEF theory via Eq. (15) in the limit of a small scalar. We point out that ξ_{\min} increases significantly with a when a is large.

We also notice that when a is from 0.01 to 1 in Eq. (35), the order of magnitude of the scalar mass m_Φ coincides with the values from the spin measurement of superradiant black holes in X-ray binaries [39]. Superradiance for black holes with a light scalar field is an interesting topic, which we will not go into detail in this paper however.

B. Numerical results of the nonlinear problem

Knowing the parameter space of ξ and a for spontaneous scalarization from the study of the linearized scalar field, it is relatively straightforward to numerically solve the group of nonlinear equations in (21). One thing that calls for attention is the numerical singularity at $\rho = 0$. To avoid it, our numerical integrations start at a small radius $\rho = \rho_{\min}$ [6]; it is also true when numerically solving the linearized scalar equation from the center. Series expansions of relevant functions at the center show that the values of the functions at $\rho = \rho_{\min}$ are the same as their values at $\rho = 0$ at least up to $O(\rho_{\min})$, but the derivatives of them take corrections at $O(\rho_{\min})$. The two derivatives used for starting numerical integrations are

$$\begin{aligned} \Phi'|_{\rho_{\min}} &= \frac{\rho_{\min}}{3W} \left(4\pi A^3 \frac{dA}{d\Phi} (\tilde{\epsilon} - 3\tilde{p}) + A^3 \frac{dA}{d\Phi} U + \frac{1}{4} A^4 \frac{dU}{d\Phi} \right) \Big|_{\rho=\rho_{\min}}, \\ \omega'|_{\rho_{\min}} &= \frac{16\pi\rho_{\min}}{5} A^4 (\tilde{\epsilon} + \tilde{p}) \omega \Big|_{\rho=\rho_{\min}}. \end{aligned} \quad (36)$$

The fact that the solutions only depend on two independent input parameters, the central pressure \tilde{p}_c and the central scalar field Φ_c , is unaltered by slightly shifting the starting point of integration.

Similar to solving the linearized scalar equation, the requirement of $\Phi \rightarrow 0$ at infinity is achieved by using the shooting method. In practice, among the two inputs, \tilde{p}_c and Φ_c , adjusting the latter fulfills the requirement more efficiently.

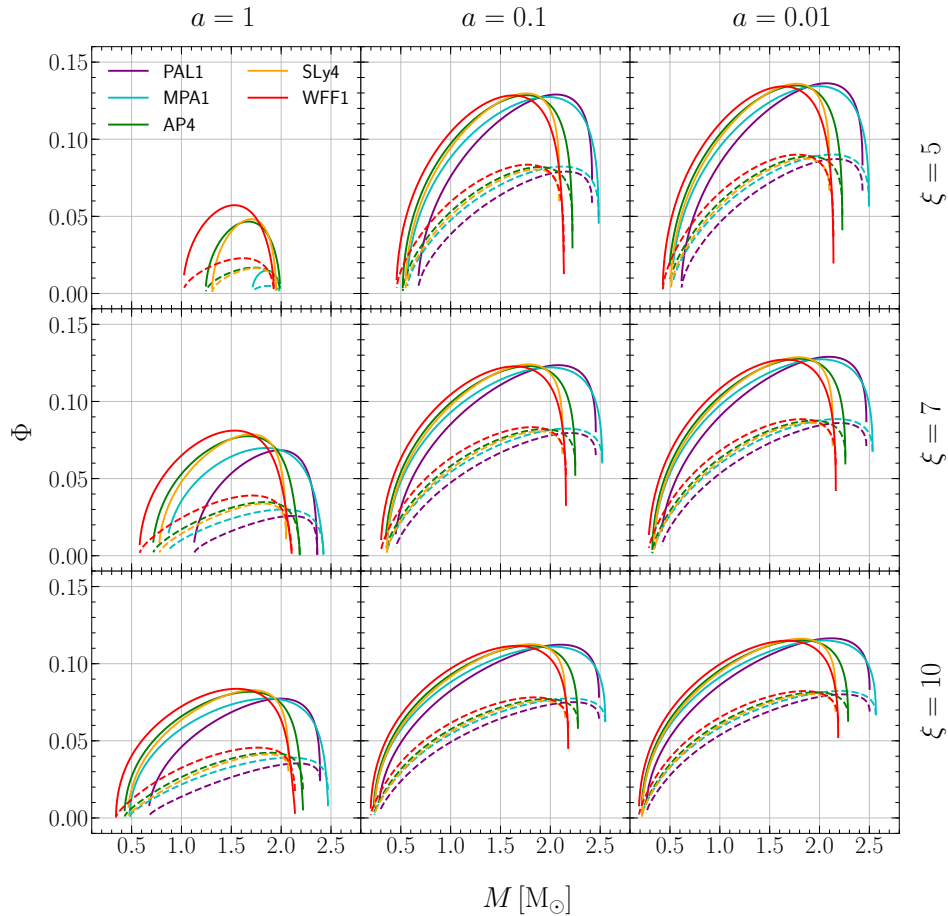


FIG. 4. The values of the scalar field at the center (solid curves) and on the surface (dashed curves) of the star versus its ADM mass M for three typical values of ξ and a . The same five EOSs as in Fig. 2 are used. Note that no solutions of spontaneous scalarization exist with the EOS PAL1 for $\xi = 5$ and $a = 1$, as ξ_{\min} is slightly greater than 5 when $a = 1$ for the EOS PAL1 (cf. Fig. 2).

Varying \bar{p}_c , on the other hand, changes rapidly the parameters of the star, i.e., its compactness and its mass.

Numerical results of spontaneous scalarization for various values of ξ and a in the regions above the curves in Fig. 2 have been obtained. Figure 3 shows example solutions of the metric components in the Jordan frame as functions of the radius r defined in Eq. (37) for NSs with $1.4 M_{\odot}$ and $2.0 M_{\odot}$.

Figures 4–6 describe characteristic quantities of NSs solved by varying the central pressure. In Fig. 4, we choose the values of the scalar field at the center and on the surface of the star to display with respect to the ADM mass, signalling the extent of spontaneous scalarization for NSs with different masses in the ST theories with three representative values of ξ and three representative values of a . The allowed interval of the ADM mass for spontaneous scalarization depends on values of ξ and a . The larger ξ is and the smaller a is, the wider range M covers for spontaneous scalarization. We point out that in Fig. 4, except for the upper left panel, unstable solutions come up when approaching the upper onset of spontaneous scalarization [10]. These unstable solutions are removed from the plots.

To compare with GR solutions, the mass-radius relation and

the change of inertia moment with respect to M are shown in Figs. 5 and 6 respectively. From the figures, we see that the deviations of scalarized NSs from their counterparts in GR grow with ξ and reduce with a in general. But for given values of ξ and a , there is always a scalarized NS having the same ADM mass and radius as its counterpart in GR. When the mass of a NS is heavier than this special mass, its radius increases once the star is scalarized, and vice versa. For this reason, a heavy (light) scalarized NS acquires a larger (smaller) moment of inertia compared to its counterpart in GR, as shown in Fig. 6.

Our plots are qualitatively consistent with the results in Refs. [10, 25, 27]. The values of the scalar field at the center of the stars obtained in Ref. [10] and the deviations from GR shown in the M - R and I - M plots in Ref. [25] are relatively larger than those in Figs. 4, 5 and 6 here. The difference is mainly from the specific forms of the nonminimal couplings used in calculation. Compared to the exponential coupling function in Eq. (13) adopted by Refs. [10, 25], the rational coupling function defined in Eq. (7) produces milder spontaneous scalarization.

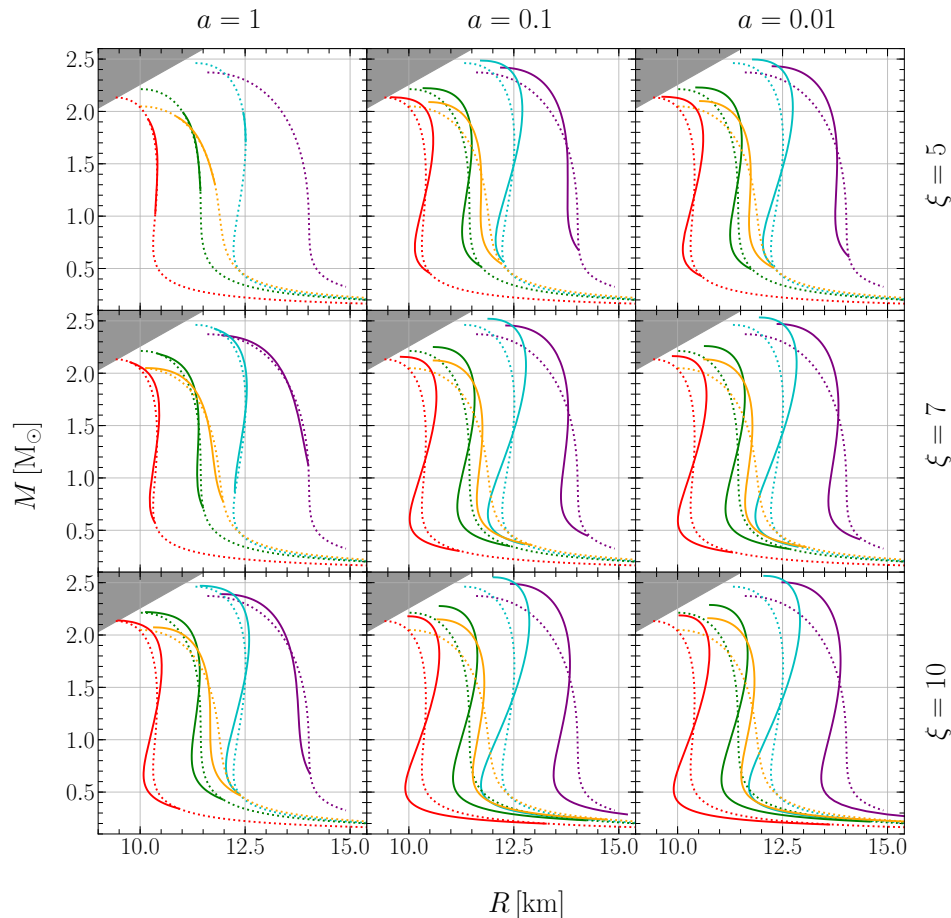


FIG. 5. Mass-radius plots for the same values of ξ and a , as well as the same set of EOSs used in Fig. 4. The solid curves are results of spontaneous scalarization, while the dotted curves are results from GR. The shaded region is $R < 3M$ for guiding purpose.

IV. APPLICATIONS

In this section we study test-particle geodesics around scalarized NSs and apply the lightlike geodesics to construct the pulse profiles of X-ray pulsars with an illustrative model.

A. Test particle geodesics

Test particles around scalarized NSs follow trajectories different from those in GR due to the distinctive metric solutions. Here we investigate the difference by analytically considering the geodesics in a general static spherical spacetime and numerically implementing several solutions of scalarized NSs as an illustration. The geodesic equation holds in the Jordan frame, so the motion of test particles will be studied using the physical metric $\tilde{g}_{\mu\nu}$.

Specifically, we define a new radial coordinate

$$r \equiv A(\varphi)\rho, \quad (37)$$

so that the line element in the Jordan frame can be obtained

from Eq. (16) as

$$d\tilde{s}^2 = A^2 ds^2 = -g(r) dt^2 + f(r) dr^2 + r^2 d\theta^2 + r^2 \sin^2 \theta (d\phi + (\omega - \Omega) dt)^2, \quad (38)$$

where f and g are related to μ and ν in Eq. (16) by

$$f = \left(\frac{d\rho}{dr}\right)^2 A^2 e^\mu, \quad g = A^2 e^\nu. \quad (39)$$

To simplify the calculation, we will drop the $(\omega - \Omega)$ term in Eq. (38) so that the metric $\tilde{g}_{\mu\nu}$ is spherically symmetric. Then, similar to the Schwarzschild spacetime, the geodesic equation is completely integrable. The spherical symmetry also allows us to take $\theta = \pi/2$, and the first integrals are

$$\begin{aligned} g \frac{dt}{d\tau} &= \tilde{E}, \\ -g \left(\frac{dt}{d\tau}\right)^2 + f \left(\frac{dr}{d\tau}\right)^2 + r^2 \left(\frac{d\phi}{d\tau}\right)^2 &= \kappa, \\ r^2 \frac{d\phi}{d\tau} &= \tilde{L}, \end{aligned} \quad (40)$$

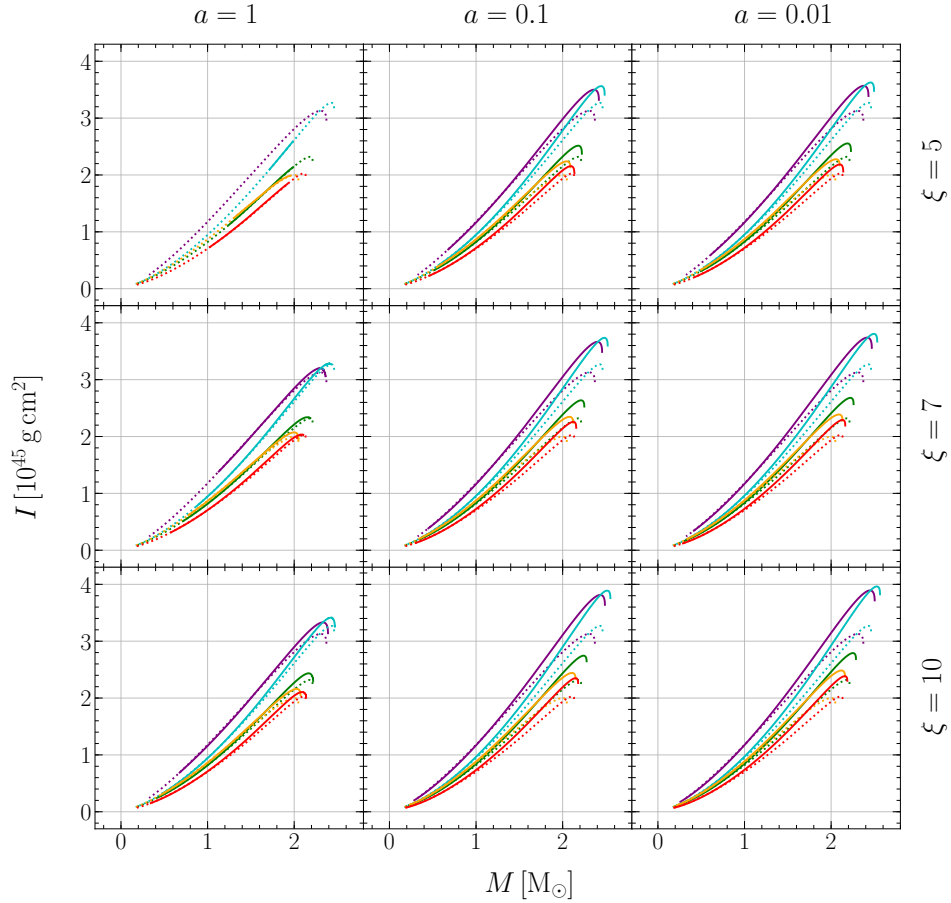


FIG. 6. The moment of inertia I versus the ADM mass M for the same values of ξ and a , as well as the same set of EOSs used in Fig. 4. The solid curves are results of spontaneous scalarization, while the dotted curves are results from GR.

TABLE I. Properties of ISCOs and the maximal values of the angle ψ defined in Fig. 8 for several scalarized NSs solved with the EOS AP4. Note that for $(\xi, a) = (5, 1)$, the ADM mass of scalarized NSs cannot reach $2M_\odot$.

Parameters			ISCO properties					Maximal ψ
(ξ, a)	$M (M_\odot)$	R (km)	r (km)	\tilde{E}	$\tilde{L} (M)$	$\frac{d\phi}{dt}$ (ms^{-1})	Grav. redshift	ψ_{\max}
GR: (0, 0)	1.40	11.42	12.4	$\frac{2\sqrt{2}}{3} \approx 0.943$	$2\sqrt{3} \approx 3.46$	9.87	0.816	$2.15 \approx 123^\circ$
(5, 0.01)	1.40	11.46	12.2	0.943	3.60	10.3	0.805	$2.13 \approx 122^\circ$
(5, 1)	1.40	11.41	12.5	0.943	3.47	9.78	0.818	$2.16 \approx 124^\circ$
(10, 0.01)	1.40	11.54	11.7	0.939	3.65	11.0	0.788	$2.11 \approx 121^\circ$
(10, 1)	1.40	11.39	13.3	0.948	3.59	9.05	0.828	$2.15 \approx 123^\circ$
GR: (0, 0)	2.00	11.00	17.7	$\frac{2\sqrt{2}}{3} \approx 0.943$	$2\sqrt{3} \approx 3.46$	6.91	0.816	$2.89 \approx 165^\circ$
(5, 0.01)	2.00	11.42	17.7	0.943	3.55	7.01	0.811	$2.69 \approx 154^\circ$
(10, 0.01)	2.00	11.63	17.2	0.941	3.60	7.36	0.800	$2.61 \approx 150^\circ$
(10, 1)	2.00	11.26	18.3	0.944	3.49	6.59	0.823	$2.78 \approx 159^\circ$

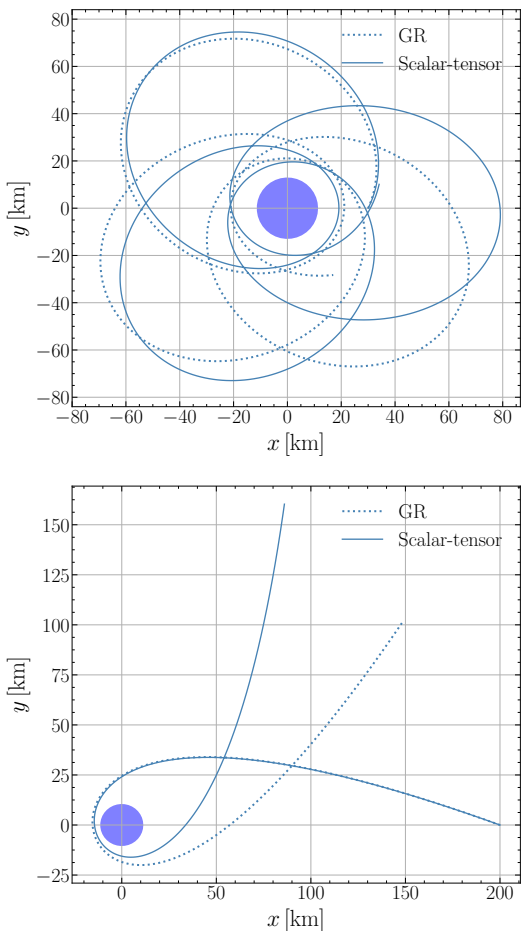


FIG. 7. Timelike test-particle orbits around a NS of $M = 1.4 M_{\odot}$ with the EOS AP4. The GR orbits are given in dotted lines for comparison. The solid disk is the NS. The Cartesian coordinates are defined as $x = r \cos \phi$, $y = r \sin \phi$. (Upper panel) $\tilde{E} = 0.98$, $\tilde{L} = 4.5M$, and (lower panel) $\tilde{E} = 1$, $\tilde{L} = 4.5M$.

where the constants \tilde{E} and \tilde{L} are respectively the specific energy and the specific angular momentum of the test particle, and the constant κ takes -1 or 0 for timelike or lightlike geodesics. The motions can be conveniently studied by eliminating $dt/d\tau$ and $d\phi/d\tau$ to define an effective radial potential

$$V_{\text{eff}}(r) \equiv -\frac{1}{2} \left(\frac{dr}{d\tau} \right)^2 = \frac{1}{2f} \left(-\frac{\tilde{E}^2}{g} + \frac{\tilde{L}^2}{r^2} - \kappa \right). \quad (41)$$

The radial coordinate r of any orbit is confined to the range where $V_{\text{eff}}(r) \leq 0$. Especially, circular orbits exist when $V_{\text{eff}} = 0$ and $dV_{\text{eff}}/dr = 0$ [40]. In addition, the circular orbit is stable (unstable) when $d^2V_{\text{eff}}/dr^2 > 0$ ($d^2V_{\text{eff}}/dr^2 < 0$), while the inflection point $d^2V_{\text{eff}}/dr^2 = 0$ determines the innermost stable circular orbit (ISCO).

Through Eq. (39), f and g can be obtained from numerical solutions of μ and ν for scalarized NSs, and then Eq. (40) can be solved numerically for given \tilde{E} and \tilde{L} . As examples, Fig. 7 shows a bound orbit and a scattering orbit around a scalarized NS, while Table I presents the properties of ISCOs for several scalarized NSs. Table I also contains the maximal values of a

quantity ψ , defined as the change of the angular coordinate ϕ for null geodesics from the surface of the star to infinity where the trajectories become straight lines. The angle ψ is illustrate in Fig. 8 in the context of the X-ray radiation from a pair of hot spots on a rotating NS (see the next subsection).

B. Effects on pulse profiles from X-ray pulsars

When radiation is emitted from a scalarized NS, the observed bolometric flux takes modification compared to the case of GR due to the difference in the bending of light by the NS spacetime. Following the method of Silva and Yunes [26], we numerically calculate the observed bolometric fluxes for the X-ray radiation emitted by a pair of hot spots on the surfaces of the NSs. Figure 8 illustrates the physical picture in consideration, and various notations are explained in the caption.

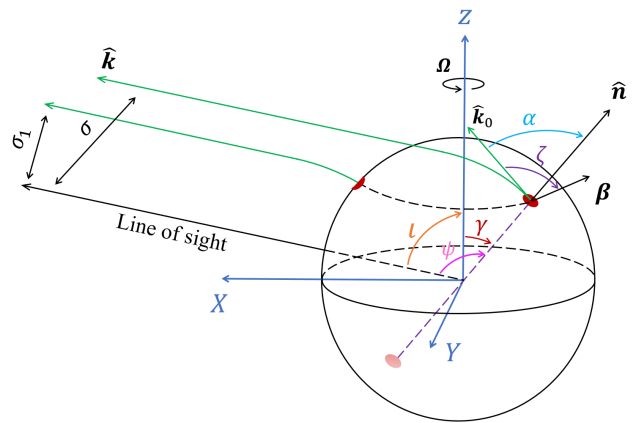


FIG. 8. Schematic illustration for the X-rays emitted from a hot spot on a rotating NS and reaching the observer at infinity. The Z-axis is along the rotation axis of the NS, while the X-axis is set in the plane formed by the Z-axis and the line of sight. The upper green curve represents a general trajectory with its initial direction along a unit vector \hat{k}_0 and its asymptotic direction along the line of sight, whose unit vector is \hat{k} . The lower green curve specifically stands for the trajectory of the ray when the hot spot is in the XZ-plane and closest to the observer. The unit vector \hat{n} is pointing along the local radial direction, and the vector β is the velocity of the hot spot in the local static frame. Five relevant angles are indicated: the angle ι between the line of sight and the Z-axis, the colatitude γ of the hot spot in the XYZ-frame, the angle ψ between the line of sight and \hat{n} , the angle α between \hat{k}_0 and \hat{n} , and the angle ζ between \hat{k}_0 and β .

We follow the assumptions in Ref. [26] in calculating the observed flux. To ease the reading, we briefly review them here. First, the radiative hot spots are assumed to have infinitesimal areas sitting oppositely on the surface of the NS at two poles. The specific intensities of the radiation at two spots are assumed to have the same dependence on the energy and the emitting direction in their locally comoving frames. For simplicity in the demonstration, the radiation is additionally presumed to be isotropic, leaving the specific intensity a

function of the energy alone. The model of isotropic radiation works if the hot spots are blackbodies and sit in vacuum. However, for realistic hot spots on the surface of a NS, the presence of a strong magnetic field and the Compton scattering in the magnetosphere of the NS generate nontrivial angular patterns of the radiation even if the hot spots themselves can be approximated as blackbodies (e.g., see Refs. [41–44]). Therefore, the isotropic assumption must be replaced by a more realistic angular distribution of the radiation when the theoretical predictions are to be confronted against data from X-ray pulsar observations [45]. Second, the trajectories of photons are assumed to follow Eq. (40) with $\kappa = 0$. In doing so, the effect from the rotation of the NS on the spacetime is neglected, namely that we have assumed a spherically symmetric curved spacetime. Also, if the X-ray pulsar lives in a binary system, we are neglecting the effect on spacetime caused by its companion star. Finally, the distance from the observer to the NS is assumed to be large enough so that it can be mathematically treated as infinity. These assumptions can be relaxed when necessary.

With the above assumptions and the relevant angles defined in Fig. 8, we summarize the derivation for the observed flux at infinity, as demonstrated in Ref. [26], into the following steps.

1. Using the specific intensity at infinity, $I(E, \hat{\mathbf{k}})$, which is a function of the observed energy E , and the unit vector $\hat{\mathbf{k}}$ along the observed direction of the ray, the observed differential flux can be expressed as

$$dF = I(E, \hat{\mathbf{k}}) dE d\Omega = I(E, \hat{\mathbf{k}}) dE \frac{\sigma d\sigma d\lambda}{D^2}, \quad (42)$$

where $d\Omega$ is the differential solid angle formed by light rays coming to the observer with the impact parameter ranging from σ to $\sigma + d\sigma$ and the azimuth angle around $\hat{\mathbf{k}}$ ranging from λ to $\lambda + d\lambda$. The distance D from the observer to the NS is assumed to be large.

2. To express Eq. (42) in terms of quantities at the emission point, the fact that the quantity I/E^3 is conserved along light rays is useful. Denoting the specific intensity in the local static frame at the emission point as $I_0(E_0, \hat{\mathbf{k}}_0)$, which is a function of the emitting energy E_0 , and the unit vector $\hat{\mathbf{k}}_0$ along the emitting direction, gravitational redshift leads to

$$I = \left(\frac{E}{E_0}\right)^3 I_0 = g^{\frac{3}{2}}(R) I_0. \quad (43)$$

The impact parameter σ is related to the angle ψ , defined as the change of the angular coordinate ϕ for null geodesics in Eq. (40) from the surface of the star to the distant observer (see Fig. 8), by integrating the trajectory equation, namely

$$\psi(\sigma) = \int_R^\infty \left| \frac{d\phi}{dr} \right| dr = \sigma \int_R^\infty \frac{\sqrt{fg}}{r^2} \frac{1}{\sqrt{1 - \frac{\sigma^2 g}{r^2}}} dr, \quad (44)$$

where the specific energy \tilde{E} and the specific angular momentum \tilde{L} of the photon in Eq. (40) have been eliminated by σ using the relation

$$\sigma = \frac{\tilde{L}}{\tilde{E}}. \quad (45)$$

Therefore, the observed differential flux in terms of the quantities at the emission point is

$$\begin{aligned} dF &= g^2(R) I_0 dE_0 \frac{\sigma(\psi) d\psi d\lambda}{D^2} \frac{d\sigma}{d\psi} \\ &= \frac{g^2(R) I_0 dE_0 dS}{D^2 R^2} \frac{\sigma(\psi) d\sigma}{\sin \psi d\psi}, \end{aligned} \quad (46)$$

where the function $\sigma(\psi)$ is the inverse of the function $\psi(\sigma)$ in Eq. (44), and $dS = R^2 \sin \psi d\psi d\lambda$ is the differential surface area in the local static frame at the emission spot.

3. Only considering the kinematic effect caused by the rotation of the NS, a local Lorentz boost is requisite for bringing I_0 , E_0 and dS into the locally comoving frame at the spot. Their transformations under a boost are (e.g., see Ref. [46])

$$dS = \delta dS', \quad E_0 = \delta E'_0, \quad I_0 = \delta^3 I'_0, \quad (47)$$

where δ is the relativistic Doppler factor, which depends on the boost speed β and the angle ζ between the boost velocity $\boldsymbol{\beta}$ and the direction of the radiation $\hat{\mathbf{k}}_0$ via [46]

$$\delta = \frac{\sqrt{1 - \beta^2}}{1 - \beta \cos \zeta}. \quad (48)$$

In our case, β and $\cos \zeta$ can be calculated by [45]

$$\begin{aligned} \beta &= \frac{R\Omega \sin \gamma}{\sqrt{-g(R)}}, \\ \cos \zeta &= -\frac{\sin \alpha \sin \iota \sin(\Omega t_0)}{\sin \psi}, \end{aligned} \quad (49)$$

where t_0 is the coordinate time when the ray is emitted and has been set to zero when the spot is closest to the observer. The angle γ is the colatitude of the hot spot; the angle α spans from the local radial direction of the spot to the direction of the radiation; and ι is the inclination angle of the distant observer (see Fig. 8). Substituting Eq. (47) into Eq. (46), we get

$$\begin{aligned} dF &= \frac{\delta^5 g^2(R) I'_0 dE'_0 dS'}{D^2 R^2} \frac{\sigma(\psi) d\sigma}{\sin \psi d\psi}, \\ &= \frac{\delta^5 g(R) I'_0 dE'_0 dS'}{D^2} \frac{\sin \alpha \cos \alpha d\alpha}{\sin \psi d\psi}, \end{aligned} \quad (50)$$

where the relation

$$\sin \alpha = \frac{\sigma \sqrt{g(R)}}{R}, \quad (51)$$

has been used to eliminate σ using α .

4. Finally, as the star rotates, the angle ψ changes according to

$$\cos \psi = \cos \iota \cos \gamma + \sin \iota \sin \gamma \cos(\Omega t_0), \quad (52)$$

which, interpreted as a function of t_0 and combined with Eq. (50), gives the relation between the observed flux dF and the emission time t_0 for given values of ι and γ . However, the observer time t , is delayed compared to t_0 by the traveling time of the photon

$$t(\sigma) - t_0 = \int_R^\infty \sqrt{\frac{f}{g}} \frac{1}{\sqrt{1 - \frac{\sigma^2 g}{r^2}}} dr, \quad (53)$$

which diverges as the trajectory extends to infinity mathematically. For our purpose, a relative time delay can be defined by

$$\begin{aligned} \delta t(\sigma) &\equiv t(\sigma) - t_0 - \int_R^\infty \sqrt{\frac{f}{g}} dr \\ &= \int_R^\infty \sqrt{\frac{f}{g}} \left(\frac{1}{\sqrt{1 - \frac{\sigma^2 g}{r^2}}} - 1 \right) dr, \end{aligned} \quad (54)$$

which turns out to be finite. Assuming the impact parameter is σ_1 when the spot is closest to the observer as shown in Fig. 8, then by resetting the observer time as $t' \equiv t(\sigma) - t(\sigma_1)$, the emission time t_0 can be expressed by the new observer time t' as

$$t_0 = t' - \delta t(\sigma) + \delta t(\sigma_1). \quad (55)$$

Now by replacing the emission time t_0 with the observer time t' using Eq. (55), the observed flux dF in Eq. (50) is a function of the observer time t' .

Following Silva and Yunes [26], we integrate Eq. (50) over dE'_0 under the isotropic assumption, and numerically calculate the normalized flux

$$F \equiv \frac{D^2 \int dF}{dS' \int I'_0 dE'_0} = \delta^5 g(R) \frac{\sin \alpha \cos \alpha d\alpha}{\sin \psi d\psi}. \quad (56)$$

Equations (50) and (56) are essentially the generalized version of the results in Ref. [26] for any static spherical spacetime.

In Fig. 9, ψ calculated with Eq. (44) and δt calculated with Eq. (54) are plotted as functions of α , for the scalarized NSs listed in Table I. In Fig. 10, by choosing two sets of (ι, γ) for the hot spots and assuming the rotation frequency of the NS to be 400 Hz, their fluxes calculated with Eq. (56) are displayed with respect to the observer time t' .

From Fig. 9, we can see that the deviations from GR become perceivable for scalarized NSs with $2 M_\odot$ as α increases from 0 to $\pi/2$. But for NSs with $1.4 M_\odot$, the deviations from GR can only be seen when the graphs are zoomed in. This is the reason why the X-ray pulse profiles for the NSs with

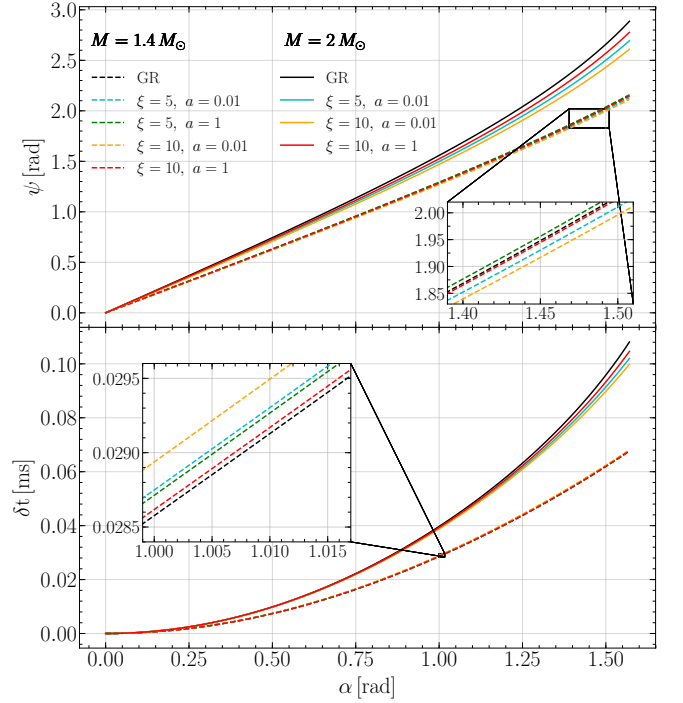


FIG. 9. (Upper panel) ψ versus α , and (lower panel) δt versus α . The solid curves are for the $2 M_\odot$ NSs in Table I, and the dashed curves are for the $1.4 M_\odot$ NSs in Table I. NSs with the same mass but different values of ξ and a are distinguished by colors. The results in GR are plotted in black for comparison.

$1.4 M_\odot$ in Fig. 10 are mostly indistinguishable. We do notice that by summing the fluxes from the spot and from the antipodal spot, the degeneracy weakens a bit (the dashed profiles in the upper right panel in Fig. 10). Another feature in the X-ray pulse profiles is that the flux from a single spot might be cut off if the spot rotates to a position where ψ calculated from Eq. (52) is greater than the maximal values presented in the last column of Table I. However, because ψ_{\max} is generally greater than $\pi/2$, when taking the pair of spots into consideration, there is no cut-off region in the profiles (right panels in Fig. 10).

V. SUMMARY

ST theories can possess distinct solutions for NSs from those of GR through spontaneous scalarization. Taking the nonminimal coupling between the scalar field and gravity from inflationary models, we study a class of specific massive ST theories described by the action (1) in this work. The field equations in both the Jordan frame and the Einstein frame are shown, and with the configuration of a slowly rotating NS the field equations are simplified to the set of ODEs in Eq. (21). A match of the theory (1) with the DEF theory with a mass term in the regime of linearized scalar is established via Eq. (15). Then the linearized scalar equation is investigated to obtain the theory parameter space for spontaneous scalarization. The

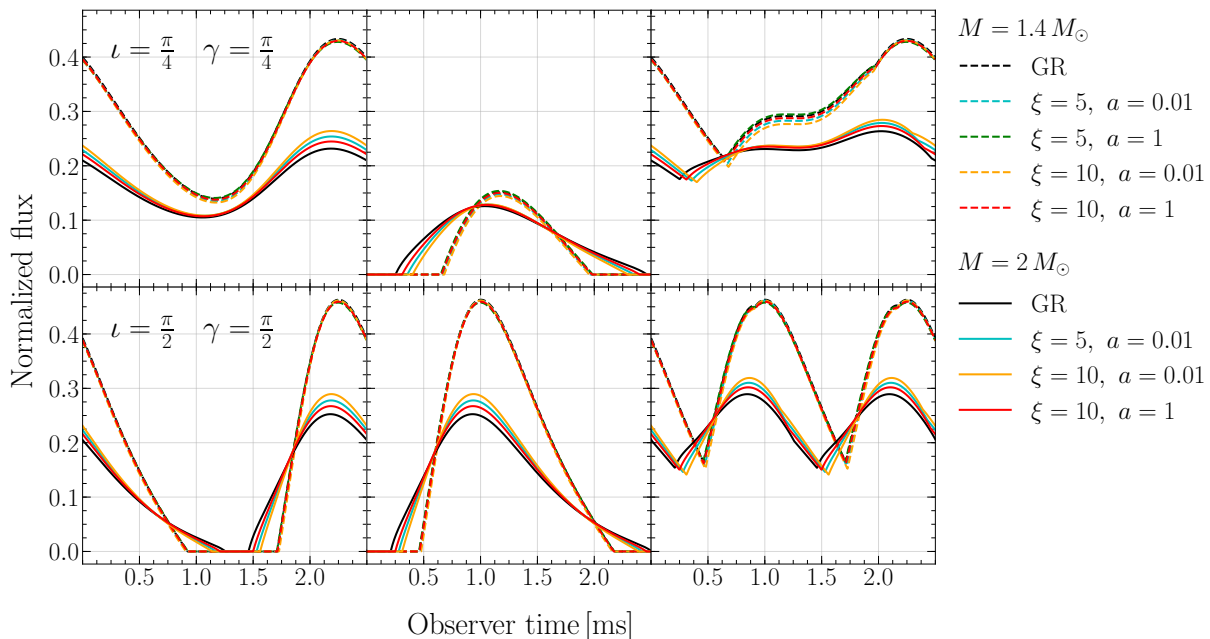


FIG. 10. The X-ray pulse profiles for NSs listed in Table I with $\iota = \pi/4$, $\gamma = \pi/4$ (upper panels) and $\iota = \pi/2$, $\gamma = \pi/2$ (lower panels). The angular frequency of the NSs is taken to be 400 Hz. (Left panels) The pulse profiles of the spots at colatitude γ . (Middle panels) The pulse profiles of the antipodal spots at colatitude $\pi - \gamma$. (Right panels) The pulse profiles of the pair of spots summed. The solid curves are for $2 M_{\odot}$ NSs, and the dashed curves are for $1.4 M_{\odot}$ NSs. NSs with the same mass but different values of ξ and a are distinguished by colors.

results, plotted in Fig. 2, are also indicative for the DEF theory with a mass term through the match in Eq. (15).

Numerical solutions for the full set of the ODEs in Eq. (21) have been obtained, and geodesics around the scalarized NSs have been calculated as an application. As preparation for putting the theory into tests, we calculated the mass-radius relation (Fig. 5), the moment-of-inertia-mass relation (Fig. 6), and the X-ray pulse profiles (Fig. 10) to compare with those predicted in GR. An interesting observation is that there is a special mass at which NSs are almost identical in the theory (1) and in GR. Though depending on the theory parameters ξ and a , as well as the EOS, the special mass for a wide range of the theory parameters and most of the EOSs that we use is around $1.5 M_{\odot}$. This makes distinguishing the theory (1) and GR difficult using observations of NSs with masses around $1.5 M_{\odot}$. In fact, due to the substantial uncertainties in measuring NS radii and moments of inertia, the theory (1) with ξ as large as 10 and a as small as 0.01 still produces M - R and I - M relations consistent with the observations as long as the EOSs used are not excluded by observations interpreted under GR.

The difficulty of distinguishing the theory (1) and GR using observations might be solved with the ongoing Neutron star Interior Composition Explorer (NICER) mission [47] as well as the revolutionary gravitational wave (GW) detecting technology. By employing sophisticated techniques during data analysis, small differences in X-ray pulse profiles might be distinguishable. Following Ref. [26], we have demonstrated constructing the X-ray pulse profile of a slowly rotating NS which possesses a general static spherical metric. To produce realistic X-ray pulse profiles for NICER to test, an integra-

tion of Eq. (50) that takes the angular pattern of the radiation into consideration is essential. The effect of NS rotation on the spacetime might also make a small difference on the pulse profile. Those are aspects worthy of future study. As for tests with GW observations from coalescences of binary NS systems, our solution of a single NS is only the prelude. A proper adaption of the post-Newtonian approximation developed for the massive Brans-Dicke theory in Ref. [48] is desired. This lies outside the scope of the current work and we leave it as a direction for future study.

ACKNOWLEDGMENTS

It is a pleasure to thank the anonymous referee for helpful comments. We are grateful to Zhoujian Cao, Kohei Inayoshi, and Jiayin Shen for discussions. This work was supported by the National Natural Science Foundation of China (11975027, 11991053, 11721303), the Young Elite Scientists Sponsorship Program by the China Association for Science and Technology (2018QNRC001), the Max Planck Partner Group Program funded by the Max Planck Society, and the High-performance Computing Platform of Peking University. It was partially supported by the Strategic Priority Research Program of the Chinese Academy of Sciences through the Grant No. XDB23010200. R.X. is supported by the Boya Postdoctoral Fellowship at Peking University.

Appendix A: Series expansion at $x = 0$ for the linearized scalar equation

Let us investigate the behavior of Φ near the center of the star if it satisfies Eq. (29) with $u = 3/2$ and y, v given by Eq. (31). Substituting the series expansion

$$\Phi = \sum_{n=0}^{\infty} \frac{\Phi_n}{n!} x^n, \quad (\text{A1})$$

into Eq. (29), and keeping in mind $\Phi_1 = 0$ due to the singular factor $2/x$ in front of Φ_x , we find

$$\begin{aligned} x^0 : \quad & \Phi_2 + 2\Phi_2 + \left(3\xi - a^2 - \frac{6\xi(3\eta - 1)}{2(1 - \eta)}\right)\Phi_0 = 0, \\ x^1 : \quad & \Phi_3 + \Phi_3 = 0, \\ x^2 : \quad & \frac{\Phi_4}{2!} - \Phi_2 + \frac{\Phi_4}{3} - \frac{1}{2!}C_2^1 z_1 \Phi_2 \\ & + (3\xi - a^2)\frac{\Phi_2}{2!} - 3\xi\left(\frac{3\eta - 1}{2(1 - \eta)}\Phi_2 - \frac{\eta}{2(1 - \eta)^2}\Phi_0\right) = 0, \\ x^3 : \quad & \frac{\Phi_5}{3!} - \Phi_3 + \frac{\Phi_5}{12} - \frac{1}{3!}C_3^1 z_1 \Phi_3 \end{aligned}$$

$$+(3\xi - a^2)\frac{\Phi_3}{3!} - \frac{\xi(3\eta - 1)}{2(1 - \eta)}\Phi_3 = 0, \quad (\text{A2})$$

and generically, we have

$$\begin{aligned} x^n : \quad & \frac{\Phi_{n+2}}{n!} - \frac{\Phi_n}{(n-2)!} + \frac{2\Phi_{n+2}}{(n+1)!} - \frac{1}{n!} \sum_{k=1}^n C_n^k z_k \Phi_{n-k+1} \\ & + (3\xi - a^2)\frac{\Phi_n}{n!} - \frac{6\xi}{n!} \sum_{k=1}^n C_n^k v_k \Phi_{n-k} = 0, \quad (\text{A3}) \end{aligned}$$

where C_n^k denotes the binomial coefficient, and z_k and v_k are the k -th derivatives of $z \equiv \left(\frac{5}{2} - v\right)x$ and v at $x = 0$. From the second equation in (31) we see that v is an even function of x , which indicates z to be odd. Therefore, the even and odd coefficients decouple in the recurrence relation of Φ_n . In addition, all the odd coefficients vanish due to $\Phi_3 = 0$, and all the even coefficients are proportional to Φ_0 through the linear recurrence relation. In conclusion, the solution of Φ near the center of the star is even and fixed up to an overall scaling constant which can be conveniently chosen as Φ_0 .

The above conclusion is drawn for the toy EOS, but it is verified to be true for realistic EOSs by observing that there is no physical solution of odd Φ directly using numerical calculation.

-
- [1] Y. Fujii and K. Maeda, *The Scalar-tensor Theory of Gravitation* (Cambridge University Press, 2007).
- [2] C. M. Will, *Theory and Experiment in Gravitational Physics* (Cambridge University Press, 2018).
- [3] T. Damour and G. Esposito-Farèse, *Class. Quant. Grav.* **9**, 2093 (1992).
- [4] E. Berti *et al.*, *Class. Quant. Grav.* **32**, 243001 (2015), [arXiv:1501.07274 \[gr-qc\]](#).
- [5] T. Damour and G. Esposito-Farèse, *Phys. Rev. Lett.* **70**, 2220 (1993).
- [6] T. Damour and G. Esposito-Farèse, *Phys. Rev. D* **54**, 1474 (1996), [arXiv:gr-qc/9602056 \[gr-qc\]](#).
- [7] G. Esposito-Farèse, *AIP Conf. Proc.* **736**, 35 (2004), [arXiv:gr-qc/0409081](#).
- [8] T. Damour, in *Physics of Relativistic Objects in Compact Binaries: From Birth to Coalescence*, Vol. 359, edited by M. Colpi, P. Casella, V. Gorini, U. Moschella, and A. Possenti (Springer, Dordrecht, 2009) p. 1, [arXiv:0704.0749 \[gr-qc\]](#).
- [9] N. Sennett, L. Shao, and J. Steinhoff, *Phys. Rev. D* **96**, 084019 (2017), [arXiv:1708.08285 \[gr-qc\]](#).
- [10] F. M. Ramazanoğlu and F. Pretorius, *Phys. Rev. D* **93**, 064005 (2016), [arXiv:1601.07475 \[gr-qc\]](#).
- [11] P. C. C. Freire, N. Wex, G. Esposito-Farèse, J. P. W. Verbiest, M. Bailes, B. A. Jacoby, M. Kramer, I. H. Stairs, J. Antoniadis, and G. H. Janssen, *Mon. Not. Roy. Astron. Soc.* **423**, 3328 (2012), [arXiv:1205.1450 \[astro-ph.GA\]](#).
- [12] J. Antoniadis *et al.*, *Science* **340**, 6131 (2013), [arXiv:1304.6875 \[astro-ph.HE\]](#).
- [13] L. Shao, N. Sennett, A. Buonanno, M. Kramer, and N. Wex, *Phys. Rev. X* **7**, 041025 (2017), [arXiv:1704.07561 \[gr-qc\]](#).
- [14] D. Anderson, P. C. C. Freire, and N. Yunes, *Class. Quant. Grav.* **36**, 225009 (2019), [arXiv:1901.00938 \[gr-qc\]](#).
- [15] J. Zhao, L. Shao, Z. Cao, and B.-Q. Ma, *Phys. Rev. D* **100**, 064034 (2019), [arXiv:1907.00780 \[gr-qc\]](#).
- [16] N. Wex, in *Frontiers in Relativistic Celestial Mechanics: Applications and Experiments*, Vol. 2, edited by S. M. Kopeikin (Walter de Gruyter GmbH, Berlin/Boston, 2014) p. 39, [arXiv:1402.5594 \[gr-qc\]](#).
- [17] L. Shao and N. Wex, *Sci. China Phys. Mech. Astron.* **59**, 699501 (2016), [arXiv:1604.03662 \[gr-qc\]](#).
- [18] L. Shao, *AIP Conf. Proc.* **2127**, 020016 (2019), [arXiv:1901.07546 \[gr-qc\]](#).
- [19] T. Damour and K. Nordvedt, *Phys. Rev. D* **48**, 3436 (1993).
- [20] L. Sampson, N. Yunes, N. Cornish, M. Ponce, E. Barausse, A. Klein, C. Palenzuela, and L. Lehner, *Phys. Rev. D* **90**, 124091 (2014), [arXiv:1407.7038 \[gr-qc\]](#).
- [21] T. A. de Pirey Saint Alby and N. Yunes, *Phys. Rev. D* **96**, 064040 (2017), [arXiv:1703.06341 \[gr-qc\]](#).
- [22] T. Anson, E. Babichev, and S. Ramazanov, *Phys. Rev. D* **100**, 104051 (2019), [arXiv:1905.10393 \[gr-qc\]](#).
- [23] P. Chen, T. Suyama, and J. Yokoyama, *Phys. Rev. D* **92**, 124016 (2015), [arXiv:1508.01384 \[gr-qc\]](#).
- [24] S. Morisaki and T. Suyama, *Phys. Rev. D* **96**, 084026 (2017), [arXiv:1707.02809 \[gr-qc\]](#).
- [25] S. S. Yazadjiev, D. D. Doneva, and D. Popchev, *Phys. Rev. D* **93**, 084038 (2016), [arXiv:1602.04766 \[gr-qc\]](#).
- [26] H. O. Silva and N. Yunes, *Phys. Rev. D* **99**, 044034 (2019), [arXiv:1808.04391 \[gr-qc\]](#).
- [27] A. S. Arapoğlu, K. Y. Ekşi, and A. E. Yükselci, *Phys. Rev. D* **99**, 064055 (2019), [arXiv:1903.00391 \[gr-qc\]](#).
- [28] K. V. Staykov, D. Popchev, D. D. Doneva, and S. S. Yazadjiev, *Eur. Phys. J. C* **78**, 586 (2018), [arXiv:1805.07818 \[gr-qc\]](#).
- [29] D. S. Salopek, J. R. Bond, and J. M. Bardeen, *Phys. Rev. D* **40**, 1753 (1989).

- [30] F. L. Bezrukov and M. Shaposhnikov, *Phys. Lett. B* **659**, 703 (2008), arXiv:0710.3755 [hep-th].
- [31] M. P. Hertzberg, *JHEP* **11**, 023 (2010), arXiv:1002.2995 [hep-ph].
- [32] J. B. Hartle, *Astrophys. J.* **150**, 1005 (1967).
- [33] E. Poisson and C. M. Will, *Gravity: Newtonian, Post-Newtonian, Relativistic* (Cambridge University Press, Cambridge, England, 2014).
- [34] J. M. Lattimer and M. Prakash, *Astrophys. J.* **550**, 426 (2001), arXiv:astro-ph/0002232 [astro-ph].
- [35] H. T. Cromartie *et al.*, *Nature Astron.* **4**, 72 (2019), arXiv:1904.06759 [astro-ph.HE].
- [36] B. Abbott *et al.* (LIGO Scientific, Virgo), *Phys. Rev. Lett.* **119**, 161101 (2017), arXiv:1710.05832 [gr-qc].
- [37] B. Abbott *et al.* (LIGO Scientific, Virgo), *Phys. Rev. X* **9**, 011001 (2019), arXiv:1805.11579 [gr-qc].
- [38] B. Abbott *et al.* (LIGO Scientific, Virgo), *Phys. Rev. Lett.* **121**, 161101 (2018), arXiv:1805.11581 [gr-qc].
- [39] R. Brito, V. Cardoso, and P. Pani, *Superradiance: Energy Extraction, Black-Hole Bombs and Implications for Astrophysics and Particle Physics*, Vol. 906 (Springer, 2015) arXiv:1501.06570 [gr-qc].
- [40] C. W. Misner, K. S. Thorne, and J. A. Wheeler, *Gravitation* (W. H. Freeman, San Francisco, 1973).
- [41] P. Meszaros, *High-energy Radiation from Magnetized Neutron Stars* (University of Chicago Press, Chicago, USA, 1992).
- [42] J. Madej, *Astrophys. J.* **376**, 161 (1991).
- [43] F. Ozel, *Astrophys. J.* **563**, 276 (2001), arXiv:astro-ph/0103227.
- [44] J. Poutanen, *AIP Conf. Proc.* **1068**, 77 (2008), arXiv:0809.2400 [astro-ph].
- [45] J. Poutanen and A. M. Beloborodov, *Mon. Not. Roy. Astron. Soc.* **373**, 836 (2006), arXiv:astro-ph/0608663.
- [46] G. B. Rybicki and A. P. Lightman, *Radiative Processes in Astrophysics* (Wiley-VCH, 2004).
- [47] P. S. Ray, Z. Arzoumanian, and K. C. Gendreau (Multiwavelength Coordination), *IAU Symp.* **337**, 187 (2017), arXiv:1711.08371 [astro-ph.HE].
- [48] J. Alsing, E. Berti, C. M. Will, and H. Zaglauer, *Phys. Rev. D* **85**, 064041 (2012), arXiv:1112.4903 [gr-qc].